Spin-polarized electron transport through helicene molecular junctions

Ting-Rui Pan,[1] Ai-Min Guo,[2,*] and Qing-Feng Sun[1,3,†]

[1]*International Center for Quantum Materials, School of Physics, Peking University, Beijing 100871, China*

[2]*Department of Physics, Harbin Institute of Technology, Harbin 150001, China*

[3]*Collaborative Innovation Center of Quantum Matter, Beijing 100871, China*

(Received 11 October 2016; revised manuscript received 29 November 2016; published 30 December 2016)

Recently, the spin-selectivity effect of chiral molecules has been attracting extensive and growing interest among the scientific communities. Here, we propose a model Hamiltonian to study spin-dependent electron transport through helicene molecules which are connected by two semi-infinite graphene nanoribbons and try to elucidate a recent experiment of the spin-selectivity effect observed in the helicene molecules. The results indicate that the helicene molecules can present a significant spin-filtering effect in the case of extremely weak spin-orbit coupling, which is three orders of magnitude smaller than the hopping integral. The underlying physics is attributed to intrinsic chiral symmetry of the helicene molecules. When the chirality is switched from the right-handed species to the left-handed species, the spin polarization is reversed exactly. These results are consistent with a recent experiment [V. Kiran *et al.*, Adv. Mater. **28**, 1957 (2016)]. In addition, the spin-filtering effect of the helicene molecules is robust against molecular lengths, dephasing strengths, and space position disorder. This theoretical work may motivate further studies on chiral-induced spin selectivity in molecular systems.

DOI: 10.1103/PhysRevB.94.235448

I. INTRODUCTION

The field of spintronics has attracted extensive attention from the physics, biology, and chemistry communities, owing to promising applications in storing and processing information [1–3]. Recent works demonstrated a spin-filtering phenomenon in a number of chiral molecules, which is termed chiral-induced spin selectivity. It was reported that both self-assembled monolayers of double-stranded DNA (dsDNA) and single dsDNA molecules can discriminate electron spin [4,5], with spin filtration efficiency exceeding 60% at room temperature. The spin-polarized currents were found in single-wall carbon nanotubes wrapped by single-stranded DNA (ssDNA) [6,7], although the ssDNA molecules cannot present the spin-filtering effect. In addition, the spin-selectivity effect was observed in a variety of α-helical proteins, like bacteriorhodopsins [8], oligopeptides [9], and photosystem I [10], as well as in other chiral polymers [11]. In our previous works, a theoretical model was put forward to interpret quantum spin transport through the dsDNA [12–14] and the α-helical protein [15,16], where the high spin filtration efficiency is caused by spin-orbit coupling (SOC) and intrinsic chiral structure. In addition, analytical expressions of the transmission coefficient and the spin polarization were obtained when electrons with arbitrary spin orientation transport through a helix-shaped potential barrier [17]. By considering leakage of electrons to side leads, spin-dependent nonunitary electron transport along a single-helical molecule was studied [18].

Notice that the aforementioned chiral molecules, such as the dsDNA molecules, the α-helical protein, and the chiral polymers, contain two helical chains at most and possess stereogenic carbon centers. In this paper, we study a different chiral molecule, helicene, which has no stereogenic carbons and contains three helical chains. Helicene is inherently chiral with nonplanar screw-shaped skeletons formed by incorporating several consecutive ortho-fused benzene rings or other (hetero)aromatics [Fig. 1(a)] [19,20]. It is usually called [N] helicene, where [N] denotes the number of aromatic rings in the helical backbone. The left-handed helical helicene and the right-handed one are, respectively, characterized by their M and P enantiomers. Since it was first synthesized, helicene and its derivatives have been produced with good yields [21,22]. Meanwhile, the helicene has potential applications such as molecular springs [23,24], chiral recognition [25–27], and organic electronic devices [28–31].

Recently, the charge transport was theoretically investigated in the helicene molecules [32,33], and the spin-polarized transport was performed in the experiment [34]. The electron transport properties of the helicene molecules under stretching or compressing along the helix axis were theoretically investigated, and a U-shaped curve of the current against the molecular pitch was observed [32]. A combination of density functional theory and tight-binding calculations showed that mechanically stretching or compressing the molecular junction, which is composed of the helicene molecules and two gold electrodes, can dramatically modify the electronic properties of the helicene molecules [33]. A tunable switching behavior of the conductance and thermopower was found with an on-off ratio of several orders of magnitude [33]. Very recently, the chiral-induced spin selectivity was demonstrated in the helicene molecules adsorbed as an oriented monolayer on a highly oriented pyrolytic graphite substrate by measuring the magnetoresistance effect [34]. It was shown that the helicene molecules can be an efficient spin filter and the spin-polarized direction was opposite between the P and M enantiomers [34]. However, to our knowledge, there is not any theoretical study on the spin-selective electron transport through the helicene molecules, and the underlying physical mechanism remains unclear.

*amguo@hit.edu.cn

†sunqf@pku.edu.cn

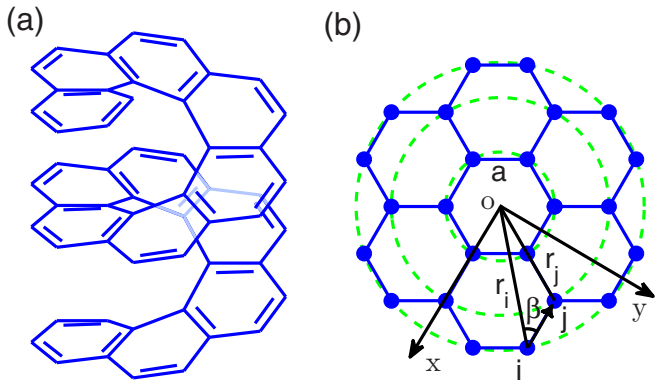

FIG. 1. (a) Schematic view of the right-handed [13] helicene molecule. Here, we consider the triple-helical model [35,36], where all the carbon atoms (substituents) construct three helices: an inner helix containing $N+1$ carbon atoms, a middle helix with $N+1$ carbon atoms, and an outer helix with $2N$ carbon atoms, where N is the number of benzene rings. The pitches of the three helical chains are the same [32]. (b) Projection of the helicene molecule into the x-y plane (the z axis is the helix axis of the molecule). The circles (sites) denote carbon atoms or substituents, which form six closely encircled regular hexagons with side length $a = 0.14$ nm in the x-y plane. r_i (r_j) is the distance from site i (j) to the helix axis, and β denotes the deviation angle of site j from the origin with respect to site i.

In this paper, we propose a model Hamiltonian to investigate the quantum spin transport through the helicene molecules which are connected to two semi-infinite graphene nanoribbons. Our results show that a relatively large spin filtration efficiency can be obtained for both right-handed and left-handed helicene molecules even in the case of extremely weak SOC, which is three orders of magnitude smaller than the hopping integral. When the chirality is switched from the right-handed species to the left-handed species, the spin polarization is reversed exactly for the helicene molecules. The spin-filtering effect of the helicene molecules can be improved by the strain effects along the helix axis. In addition, the helicene molecules remain an efficient spin filter for different molecular lengths, dephasing strengths, and space position disorder. This work may motivate further studies on the spin transport along chiral molecular systems and speed up the process for applying chiral molecules into spintronic devices.

The rest of this paper is organized as follows. In Sec. II, we propose a model Hamiltonian with parameters presented and introduce the calculation method. In Sec. III, we investigate the conductance and the spin polarization under various parameter values. Then, the space position disorder is taken into account. Finally, the results are summarized in Sec. IV.

II. MODEL AND METHOD

The spin-dependent charge transport along the helicene molecular junctions, illustrated in Fig. 1, can be described by the following Hamiltonian:

$$\mathcal{H} = \mathcal{H}_{\rm mol} + \mathcal{H}_{\rm so} + \mathcal{H}_{\rm lead} + \mathcal{H}_d. \tag{1}$$

Here, $\mathcal{H}_{\rm mol} = \hat{\mathbf{p}}^2/2m + V$ includes the kinetic and potential energies V of the electrons, with $\hat{\mathbf{p}}$ being the momentum operator and m being the electron effective mass. The second term, $\mathcal{H}_{\rm so} = (\hbar/4m^2c^2)\nabla V \cdot (\hat{\sigma} \times \hat{\mathbf{p}})$, is the SOC Hamiltonian, where $\hbar$ is the reduced Plank constant, c is the speed of light, and $\hat{\sigma} = (\sigma_x, \sigma_y, \sigma_z)$, with $\sigma_{x,y,z}$ being the Pauli matrices. The third term, $\mathcal{H}_{\rm lead}$, represents left and right leads and their couplings to the helicene molecule, while the fourth term, $\mathcal{H}_d$, denotes dephasing processes.

We consider that the electronic wave function ψ_i decays exponentially with the distance, i.e., $\psi_i \sim e^{-l_i/\lambda}$, as expected from the quantum transport in the helicene molecules [33]. The parameter l_i is the distance from site i, and λ is the decay exponent. On the basis of site representation constructed by all the carbon atoms (substituents), the Hamiltonian $\mathcal{H}_{\rm mol}$ can be expressed as

$$\mathcal{H}_{\rm mol} = \sum_i \varepsilon_i c_i^\dagger c_i + \sum_{\langle ij \rangle} t_{ij} c_i^\dagger c_j, \tag{2}$$

where $c_i^\dagger = (c_{i\uparrow}^\dagger, c_{i\downarrow}^\dagger)$ is the creation operator of site i in the helicene molecule. $\varepsilon_i = \langle \psi_i | \mathcal{H}_{\rm mol} | \psi_i \rangle$ is the on-site energy, and $t_{ij} = \langle \psi_i | \mathcal{H}_{\rm mol} | \psi_j \rangle$ is the hopping integral between sites i and j. By integrating t_{ij} along the straight line between sites i and j, one obtains $t_{ij} = te^{-(l_{ij}-l)/\lambda}$, where the hopping integral is t when the distance is l. Here, $l_{ij} = \sqrt{\bar{l}_{ij}^2 + (h\Delta\varphi/2\pi)^2}$ is the distance between sites i and j, $\bar{l}_{ij} = \sqrt{r_i^2 + r_j^2 - 2r_i r_j \cos(\Delta\varphi)}$, h is the pitch of the helicene molecule, $\Delta\varphi = \varphi_j - \varphi_i$, and r_i is the distance from site i to the helix axis, with φ_i being the azimuth angle of site i. In Eq. (2) $\langle \cdots \rangle$ represents the nearest-neighbor sites. Notice that the dependence of t_{ij} on l_{ij} is similar to the Slater-Koster scheme.

Analogously, the SOC Hamiltonian can be obtained by calculating $\langle \psi_i | \mathcal{H}_{\rm so} | \psi_j \rangle$ and is written as

$$\begin{aligned}\mathcal{H}_{\rm so} = \sum_{\langle ij \rangle} i s_{ij} c_i^\dagger \frac{r_i}{a} \Bigg[& \sigma_x \sin\theta_{ij} \left(\frac{\sin\beta \sin\varphi_j}{\sin(\beta + \Delta\varphi)} + \sin\varphi_i \right) \\ & - \sigma_y \sin\theta_{ij} \left(\frac{\sin\beta \cos\varphi_j}{\sin(\beta + \Delta\varphi)} + \cos\varphi_i \right) \\ & + 2\sigma_z \cos\theta_{ij} \sin\beta \Bigg] c_j. \end{aligned} \tag{3}$$

Here, $s_{ij} = se^{-(l_{ij}-l)/\lambda}$ is the SOC strength between sites i and j, and $\theta_{ij} = \arcsin(h\Delta\varphi/2\pi l_{ij})$ denotes the space angle between the vector from site i to site j and the x-y plane, where the SOC strength is s when the distance is l. The deviation angle of site j from the origin with respect to site i in the x-y plane is denoted by $\beta = \delta \arccos[(r_i^2 + \bar{l}_{ij}^2 - r_j^2)/2r_i\bar{l}_{ij}]$, where $\delta = 1$ for $\Delta\varphi \geqslant 0$ and $\delta = -1$ for $\Delta\varphi < 0$. We stress that the SOC Hamiltonian (3) of the helicene molecules exists not only within a certain helical chain but also between two different helical chains due to the special structure of the helicene molecules (Fig. 1). This is different from the dsDNA [12–14], the α-helical protein [15,16], and the single-helical molecule [18], where the SOC Hamiltonian appears in only a specific helical chain.

The lower and upper hexagons of the helicene molecules are connected to two semi-infinite graphene nanoribbons, which are respectively defined as the left and right leads, and the

Hamiltonian $\mathcal{H}_{\rm lead}$ can be expressed as

$$\mathcal{H}_{\rm lead} = \sum_{\mu,i} \varepsilon_i a^\dagger_{\mu i} a_{\mu i} + \sum_{\mu,\langle ij\rangle} t_{ij} a^\dagger_{\mu i} a_{\mu j} + \sum_{\mu,\langle ij\rangle} (t_{ij} a^\dagger_{\mu i} c_j + \text{H.c.}), \quad (4)$$

where $\mu = L, R$ denotes the left and right leads. The first two terms are the Hamiltonians of the left and right leads, which are similar to the Hamiltonian of $\mathcal{H}_{\rm mol}$. The last term is the couplings between the leads and the molecule, where one needs to note that $a^\dagger_{\mu i}$ and c_j denote only the terminal sites of leads and the molecule, respectively. The electrons transmitted through the helicene molecules may experience inelastic scatterings with, e.g., the phonons, the counterions, and the impurities, which will give rise to the loss of the phase memory of the electron. Actually, the presence of the decoherence in helicene molecules has been clearly indicated in previous work [33]. The phase-breaking processes can be simulated by connecting each site of the helicene molecules to one of Büttiker's virtual leads [12,15,16], of which the Hamiltonian is expressed as

$$\mathcal{H}_d = \sum_{i,k} (\varepsilon_{ik} d^\dagger_{ik} d_{ik} + t_d d^\dagger_{ik} c_i + \text{H.c.}), \quad (5)$$

where $d^\dagger_{ik} = (d^\dagger_{ik\uparrow}, d^\dagger_{ik\downarrow})$ is the creation operator of mode k in the virtual lead i and t_d is the coupling between the molecule and the virtual lead.

According to the Landauer-Büttiker (LB) formula, the current of the qth real or virtual lead with spin $s = \uparrow, \downarrow$ is written as [37,38]

$$I_{qs} = (e^2/h) \sum_{m,s'} T_{qs,ms'}(V_m - V_q), \quad (6)$$

where V_q is the voltage of the qth lead and

$$T_{qs,ms'}(E) = \text{Tr}[\Gamma_{qs} \mathbf{G}^r \Gamma_{ms'} \mathbf{G}^a] \quad (7)$$

is the transmission coefficient from the mth lead with spin s' to the qth lead with spin s. The Green's function is $\mathbf{G}^r(E) = [\mathbf{G}^a(E)]^\dagger = [E\mathbf{I} - \mathbf{H}_{\rm mol} - \mathbf{H}_{\rm so} - \sum_{qs} \Sigma^r_{qs}]^{-1}$, and the linewidth function is $\Gamma_{qs}(E) = i[\Sigma^r_{qs} - \Sigma^a_{qs}]$, where E is the incident electron energy (Fermi energy) and Σ^r_{qs} is the retarded self-energy because of the coupling to the qth lead. For the real left/right lead, $\Sigma_{\rm L/Rs}$ can be calculated numerically; however, for the virtual leads, $\Sigma^r_{qs} = -i\Gamma_d/2 = -i\pi\rho_d t_d^2$, with Γ_d being the dephasing parameter and ρ_d being the density of states of the leads. Under the boundary condition that the net current through each virtual lead is zero, their voltages can be obtained from the LB formula by applying a small external bias $V_{\rm b}$ between the left and right leads, with $V_{\rm L} = V_{\rm b}$ and $V_{\rm R} = 0$. Finally, the conductance of the right lead with spin s can be obtained as

$$G_s = (e^2/h) \sum_{m,s'} T_{{\rm R}s,ms'} V_m / V_{\rm b}. \quad (8)$$

The spin polarization is defined as

$$P_s = (G_\uparrow - G_\downarrow)/(G_\uparrow + G_\downarrow). \quad (9)$$

For the helicene molecules, all the carbon atoms construct three helical chains with the same pitch of $h = 0.45$ nm, and their projection on the x-y plane is precisely six closely encircled regular hexagons with a side length of $a = 0.14$ nm. In the following numerical calculation, the molecular length is chosen as $N = 20$, where N denotes the number of benzene rings. The distance parameter is set as $l = 0.142$ nm, and the hopping integral t is taken as the energy unit. The on-site energy is set to $\varepsilon_i = 0$ without loss of generality, and the SOC strength and the dephasing strength are $s = 0.003t$ and $\Gamma_d = 0.01t$, respectively. Note that for the helicene molecules, each site denotes a single carbon atom, and the hopping integral t between two nearest-neighbor carbon atoms is quite large (about 2.7 eV). Consequently, the ratio of the SOC strength s to the hopping integral t is much smaller in the helicene molecules than that in the dsDNA [12–14] and the α-helical protein [15,16]. The decay exponent is $\lambda = 0.133$ nm [33]. The values of all these parameters will be used throughout the paper except for specific annotation in the figures.

III. RESULTS AND DISCUSSIONS

Figure 2(a) shows the spin-up conductance $G_\uparrow$ (blue solid line) and spin-down conductance $G_\downarrow$ (red dashed line) of the right-handed helicene molecule as a function of Fermi energy E. By inspecting Fig. 2(a), one can see several distinct features. (i) Two transmission bands of nonzero conductance appear in the energy spectrum, separated by a band gap. The conductances can be larger than e^2/h at specific energy ranges, indicating that there exist two transmission modes around these energy ranges. (ii) Both $G_\uparrow$ and $G_\downarrow$ present

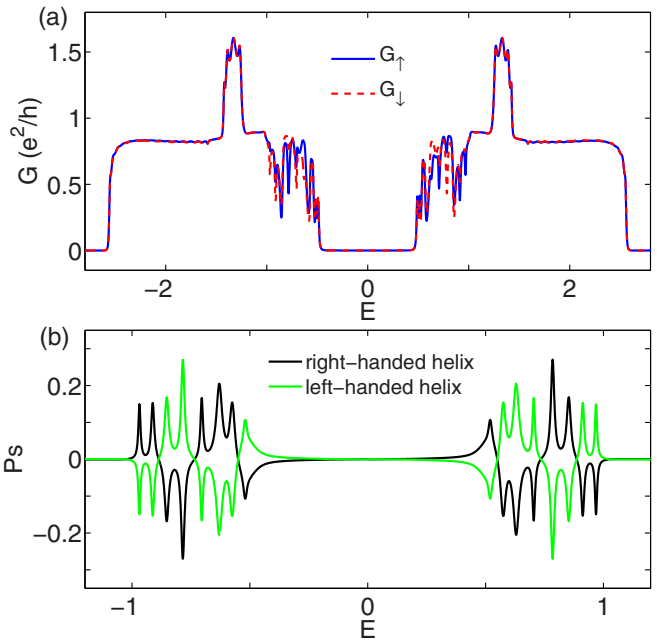

FIG. 2. (a) Energy-dependent spin-up conductance $G_\uparrow$ (blue solid line) and the spin-down one $G_\downarrow$ (red dashed line) for the right-handed helicene molecule. (b) Spin polarization P_s vs Fermi energy E for the right-handed helicene molecule (black solid line) and for the left-handed one (green solid line).

dramatic oscillating behavior when the energy of nonzero conductance is close to the band gap. (iii) The two curves of $G_\uparrow - E$ and $G_\downarrow - E$ are mirror images of each other about the line $E = 0$, i.e., $G_\uparrow(E) = G_\downarrow(-E)$. This equality originates from the electron-hole symmetry; namely, the Hamiltonian in Eq. (1) remains the same by performing the transformation $c_{i\uparrow} \to (-1)^i c^\dagger_{i\downarrow}$ and $c_{i\downarrow} \to (-1)^{i+1} c^\dagger_{i\uparrow}$. (iv) More importantly, when the Fermi energy is close to the band gap, the spin-up conductance is different from the spin-down conductance owing to the chirality of the helicene molecule. As a result, the spin polarization is nonzero [see the black solid line in Fig. 1(b)], and the helicene molecule can act as a spin filter, which is consistent with the recent experimental result [34].

Figure 2(b) plots the spin polarization P_s vs the Fermi energy E for both the right-handed and left-handed helicene molecules, where two bands of nonzero P_s can be found in the energy spectrum. It clearly appears that the spin polarization can achieve the value 27% for both the helicene molecules, which is comparable to the experimental result [34]. The spin polarization exhibits significant oscillations by varying the Fermi energy and forms peaks and valleys in the energy spectrum because of the quantum interference effects. The positive (negative) P_s implies that the spin-polarized direction is parallel (antiparallel) to the positive z axis. In particular, each curve of $P_s - E$ possesses central symmetry with respect to the point (0,0), namely, $P_s(E) = -P_s(-E)$. This equality arises from the aforementioned electron-hole symmetry and is independent of the molecular chirality. Notice that the right-handed helicene molecule is transformed into the left-handed one under the reflection operation, where the angles are changed from β to $-\beta$ and φ_i to $-\varphi_i$, with the other model parameters unchanged. Then, the spin-up and spin-down conductances exchange with each other when the right-handed helicene molecule is switched into the left-handed one. Consequently, the spin polarization is reversed exactly, i.e., $P_s(\beta,\varphi_i) = -P_s(-\beta, -\varphi_i)$ [Fig. 2(b)], which is in good agreement with the experiment [34] and previous theoretical works [12,15].

In order to demonstrate the physical origin of large spin polarization, we consider the limit case in which the pitch satisfies $h = 0^+$ and thus the angle is $\theta_{ij} = 0^+$. Notice that the helicene molecules are still chiral in this limit case. In this situation, the SOC Hamiltonian (3) is reduced to $\mathcal{H}_{\rm so} = \sum_{\langle ij\rangle} 2is_{ij}\frac{r_i}{a}\sin\beta c^\dagger_i \sigma_z c_j$. Then, the Hamiltonian of the helicene molecules, Eqs. (2) and (3), can be simplified as $\sum_{\langle ij\rangle} t_{ij} c^\dagger_i c_j + \mathcal{H}_{\rm so} = \sum_{\langle ij\rangle,s} \tilde{t}_{ij} e^{is\phi_{ij}} c^\dagger_{is} c_{js}$. Here, $s = \uparrow(+)$ and $\downarrow(-)$ represent spin up and spin down, respectively, $\tilde{t}_{ij} = \sqrt{t^2_{ij} + |2s_{ij}\frac{r_i}{a}\sin\beta|^2}$, and $\phi_{ij} = \arccos t_{ij}/\tilde{t}_{ij}$. It is now clear that the Hamiltonian of the helicene molecules is described by a spin-dependent phase ϕ_{ij}, which is similar to the case found in the quantum-dot system [39,40]. Then, we consider a simple system which consists of two transport pathways. In the presence of only the first-order tunneling process, the transmission coefficient is $T_s = |t_1 + t_2 e^{i\Delta\phi_{\rm pathway} + s\Delta\phi_{\rm soc})}|^2 = |t_1|^2 + |t_2|^2 + 2|t_1 t_2|\cos(\Delta\phi_{\rm pathway} + s\Delta\phi_{\rm soc})$. Here, t_1 and t_2 are the transmission amplitudes through pathways 1 and 2, respectively, $\Delta\phi_{\rm pathway}$ is the phase difference between the two pathways, and $\Delta\phi_{\rm soc}$ is the difference of the SOC phase between the two pathways. It is obvious that $T_\uparrow \neq T_\downarrow$ usually,

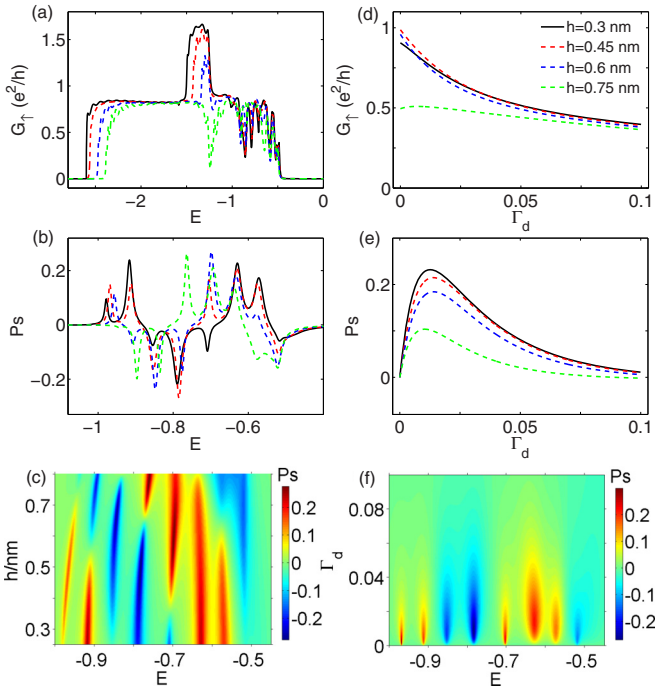

FIG. 3. (a) Spin-up conductance $G_\uparrow$ vs Fermi energy E and (b) spin polarization P_s vs E for different helicene molecules with various pitches h. (d) $G_\uparrow$ vs dephasing parameter Γ_d and (e) P_s vs Γ_d for different pitches by fixing $E = -0.63$. The top four panels have the same pitches, which are illustrated in (d). Two-dimensional plot of P_s vs (c) E and h and vs (f) E and Γ_d.

and subsequently, the spin-selectivity effect can occur in this system containing two transport pathways. We would like to point out the following two points: (i) If all the high-order tunneling processes (the electron reflected back and forth in the system) are considered, the total transmission coefficient will satisfy $T_\uparrow = T_\downarrow$. This is attributed to the so-called phase-locking effect in the two-terminal system, which arises from the current conservation and the time-reversal invariance [12,41]. However, for the multiterminal system or in the presence of the dephasing, since the high-order tunneling processes are strongly suppressed and the first-order tunneling process dominates, the spin-selectivity effect will appear. (ii) For the one-pathway system, since $T_\uparrow = |t_1 e^{i\phi_{\rm soc}}| = |t_1 e^{-i\phi_{\rm soc}}| = T_\downarrow$, the spin-polarized transport cannot occur [12,15]. As a result, multiple transport pathways are important for the emergence of the spin-selectivity effect. For the helicene molecules, the SOC Hamiltonian exists both within a single helical chain and between two different helical chains, as discussed above. This indicates that there are multiple transport pathways with various SOC phases in the helicene molecules, which leads to high spin polarization even for very small SOC strength.

The structure of the helicene molecules is flexible along the helix axis, and hence, they may serve as a molecular spring. In the following, we investigate the spin transport properties of the right-handed helicene molecule by stretching the molecule along the helix axis. Figures 3(a) and 3(b) display, respectively, spin-up conductance $G_\uparrow$ vs E and spin polarization P_s vs E for the helicene molecule by taking into account different pitches h. Here, for clarity, the numerical results are shown only in the

region of $E < 0$, and similar results can be observed for $E > 0$ as well. It can be seen from Fig. 3(a) that by increasing h, both the transmission band and the energy range of $G_\uparrow > e^2/h$ become narrower, where their left boundaries are closer to $E = 0$ and the right ones remain almost unchanged. This originates from the fact that the nearest-neighbor distance is increased, and then the hopping integral declines, which is induced by the strain effects. In addition, the maximum value of $G_\uparrow$ diminishes, and by further increasing h, the bump of $G_\uparrow > e^2/h$ can turn into the valley [see the green dashed line in Fig. 3(a)]. An analogous phenomenon can also be observed in the curves of $P_s - E$ where the width of nonzero P_s is decreased by increasing h [Fig. 3(b)]. However, the oscillation behavior remains in the energy spectrum, regardless of the pitch h. This is further demonstrated in Fig. 3(c), where the spin polarization is plotted as a function of E and h. In particular, the spin filtration efficiency is quite large for all investigated values of h and can be slightly enhanced by the strain effects. For instance, the spin polarization can reach 24% for $h = 0.3$ nm and 27% for $h = 0.6$ nm. This is attributed to the competing effect between the space angle θ_{ij} and the SOC s_{ij} under stretching in which s_{ij} decreases but θ_{ij} increases. In addition, it is interesting to notice that the positions of the maximum values of P_s remain almost the same and the sign of P_s can be reversed by the strain effects; that is, the spin-polarized direction can be changed from the positive (negative) z direction to the negative (positive) one.

Then, we study the dephasing effects on the spin transport properties of the right-handed helicene molecules. Figures 3(d) and 3(e) show, respectively, spin-up conductance $G_\uparrow$ vs the dephasing strength Γ_d and spin polarization P_s vs Γ_d for the helicene molecules by fixing $E = -0.63$, where the different curves denote various pitches h. In the presence of the dephasing, the electrons experience inelastic scatterings from each site of the molecule while transmitting through the system. The larger the dephasing strength is, the stronger scatterings the electrons suffer. As a result, the conductance is gradually declined by increasing Γ_d in general, as illustrated in Fig. 3(d). Nevertheless, in some situations, the conductance can be slightly enhanced in the regime of weak dephasing [see the green dashed line in Fig. 3(d)].

In contrast, the dependence of spin polarization P_s on the dephasing strength Γ_d is quite different. One can see from Fig. 3(e) that the behavior of P_s vs Γ_d is not monotonic. In each curve, there exists a crossover Γ_d^c of the dephasing strength, showing that the spin filtration efficiency increases with Γ_d when $\Gamma_d < \Gamma_d^c$, whereas it decreases by further increasing Γ_d when $\Gamma_d > \Gamma_d^c$, regardless of h. This nonmonotonic behavior is further illustrated in Fig. 3(f), where the spin polarization is displayed as a function of E and Γ_d. The underlying physics arises from two competing effects of the dephasing [12,15,42]. On the one hand, in the presence of the dephasing, each site of the helicene molecule is contacted by one of Büttiker's virtual leads, as discussed above. Consequently, the two-terminal helicene molecular system is changed into the multiterminal one. This role of the dephasing gives rise to the spin-filtering phenomenon and dominates in the weak-dephasing regime. Then, the spin filtration efficiency is enhanced by increasing Γ_d when the dephasing strength is small, irrespective of the Fermi energy E. On the other hand, the dephasing leads to the loss of phase memory of the electrons and, consequently, diminishes the spin polarization. The larger the dephasing strength is, the greater the loss of the phase memory is. Therefore, this role of the dephasing competes with the first one and becomes important in the strong-dephasing regime. Then, the spin polarization decreases with increasing Γ_d when Γ_d is large.

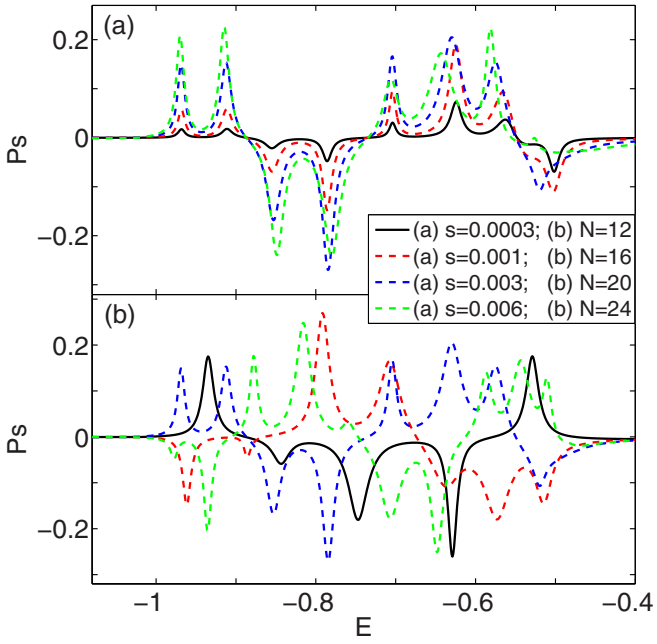

FIG. 4. Energy-dependent spin polarization P_s for the helicene molecule by considering (a) various SOC strengths s and (b) different molecular lengths N.

Next, we study the spin transport properties of the helicene molecules by considering various SOC strengths and molecular lengths. Figure 4(a) presents spin polarization P_s vs E for several SOC strengths s. It clearly appears that although the oscillating behavior persists in the energy spectrum, the absolute value of P_s and the width of the peaks as well as the valleys tend to increase with s. In other words, the spin filtration efficiency can be enhanced by increasing s since the SOC is the driving force of the spin-filtering effect in the helical molecular systems. Especially, the spin filtration efficiency remains significant in the case of extremely small SOC strength, achieving 7% for $s = 0.0003$, which is four orders of magnitude smaller than the hopping integral. Figure 4(b) displays P_s vs E for the helicene molecules with different molecular lengths N by fixing $s = 0.003$. It clearly shows that the helicene molecule acts as an efficient spin filter, with spin polarization exceeding 22% for all the investigated molecular lengths. In addition, the oscillating behavior persists, and the total number of peaks and valleys increases with increasing N because of the increment of the electronic states. Nevertheless, the positions of the peaks and the valleys depend on N, and the spin-polarized direction can be reversed by increasing N. This is different from previous works on the dsDNA molecule [4,12], the α-helical protein [9,15], and the single-helical molecule [18].

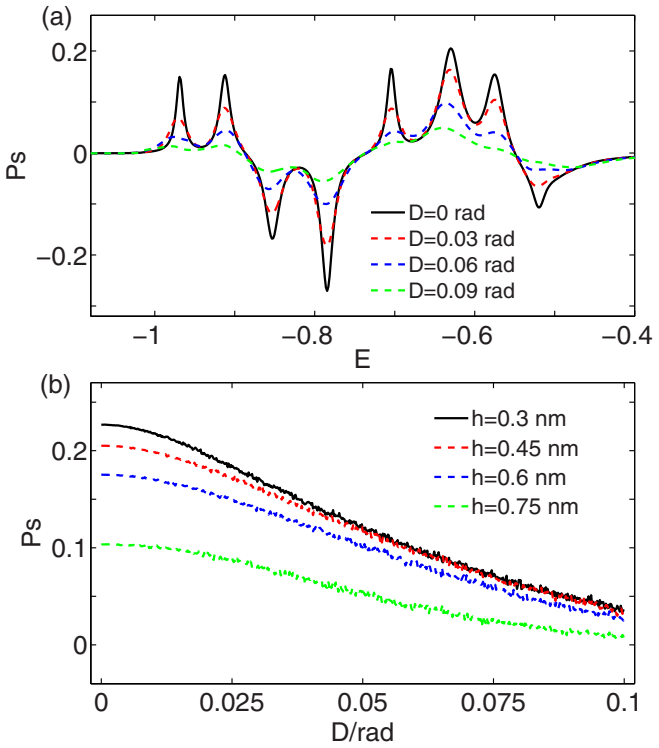

FIG. 5. (a) P_s as a function of E with different disorder strengths D of the azimuth angle. (b) P_s vs D for various pitches at $E = -0.63$. All the results are obtained by averaging over 10^3 disorder configurations.

Finally, we study the robustness of the spin-filtering effect against the disorder. Here, we consider only space position disorder, and similar results can also be observed by taking into account on-site energy disorder. At nonzero temperatures, each carbon atom will deviate from its equilibrium position because of thermal structural fluctuations. In this situation, the azimuth angle will be changed and become random. Then, the space position disorder occurs and may be reasonably simulated by incorporating a random variable d_i into every φ_i, where d_i is uniformly distributed within the range $[-D/2, D/2]$ and D is the disorder strength. Here, the results are numerically calculated from 10^3 disorder configurations for a specific value of D, and we assume that all the carbon atoms always locate at the three helices (Fig. 1). Figure 5(a) plots the spin polarization P_s vs the Fermi energy E with four values of D, while Fig. 5(b) shows P_s vs D at $E = -0.63$ by considering four different pitches h. We clearly see that both the oscillating amplitude of P_s and the spin filtration efficiency decrease with increasing D in general due to the disorder-induced Anderson localization effect. However, the spin-filtering effect of the helicene molecules is robust against the space position disorder. For example, when $D = 0.09$ rad, the spin polarization can achieve 5.5% [Fig. 5(a)]. When $D = 0.03$ rad, the spin polarization can reach 17.1%, 15.9%, 13.9%, and 8.1% for $h = 0.3$, 0.45, 0.6, and 0.75 nm, respectively [Fig. 5(b)]. From the above discussions, we demonstrate that the spin-filtering effect of the helicene molecules is robust against the space position disorder.

On the basis of the model Hamiltonian with considerably weak SOC, a relatively large spin polarization of 27% is obtained. In addition, our results indicate that the spin polarization of the right-handed helicene molecules is reversed in relation to that of the left-handed ones, which is in good agreement with the experiment [34]. Notice that the maximal spin polarization value is less than the experimental result [34]. This may be attributed to the following reasons. (i) The helicene molecules used in the experiment contain propyl group substituents, which could result in non-nearest-neighbor hopping. Here, we consider only the nearest-neighbor hopping. (ii) The large spin polarization is observed at considerably large bias voltages in the experiment. In our study, the conductances and the spin polarization are calculated under infinitely small bias voltage.

IV. CONCLUSIONS

In summary, we propose a model Hamiltonian to explore spin-dependent electron transmission along helicene molecules which are contacted by semi-infinite graphene nanoribbons. Our results reveal that the helicene molecules can present a pronounced spin-filtering phenomenon owing to the chiral symmetry, which is consistent with the recent experiment [34]. The spin filtration efficiency of the helicene molecules can be larger than 27% in the case of very weak spin-orbit coupling, which is three orders of magnitude smaller than the hopping integral. The spin-filtering effect can be slightly improved by stretching the helicene molecules along the helix axis. Additionally, the helicene molecules still possess large spin polarization by considering different molecular lengths, dephasing strengths, and space position disorder. When the chirality of the helicene molecules is switched from the right-handed species to the left-handed one, the spin polarization is reversed exactly. Our theoretical work may motivate further experimental and theoretical studies on chiral-induced spin selectivity in molecular systems and may help in designing spintronic devices by applying chiral molecules.

ACKNOWLEDGMENTS

This work was supported by NBRP of China (2015CB921102); NSF China under Grants No. 11274364, No. 11504066, and No. 11574007; and FRFCU China under Grant No. AUGA5710013615.

[1] I. Žutić, J. Fabian, and S. Das Sarma, Rev. Mod. Phys. **76**, 323 (2004).
[2] A. Fert, Rev. Mod. Phys. **80**, 1517 (2008).
[3] R. Naaman and D. H. Waldeck, Annu. Rev. Phys. Chem. **66**, 263 (2015).
[4] B. Göhler, V. Hamelbeck, T. Z. Markus, M. Kettner, G. F. Hanne, Z. Vager, R. Naaman, and H. Zacharias, Science **331**, 894 (2011).

[5] Z. Xie, T. Z. Markus, S. R. Cohen, Z. Vager, R. Gutierrez, and R. Naaman, Nano Lett. **11**, 4652 (2011).
[6] G. S. Diniz, A. Latgé, and S. E. Ulloa, Phys. Rev. Lett. **108**, 126601 (2012).
[7] K. M. Alam and S. Pramanik, Adv. Funct. Mater. **25**, 3210 (2015).
[8] D. Mishra, T. Z. Markus, R. Naaman, M. Kettner, B. Gohler, H. Zacharias, N. Friedman, M. Sheves, and C. Fontanesi, Proc. Natl. Acad. Sci. USA **110**, 14872 (2013).
[9] M. Kettner, B. Göhler, H. Zacharias, D. Mishra, V. Kiran, R. Naaman, C. Fontanesi, D. H. Waldeck, S. Sęk, J. Pawłowski, and J. Juhaniewicz, J. Phys. Chem. C **119**, 14542 (2015).
[10] I. Carmeli, K. S. Kumar, O. Heifler, C. Carmeli, and R. Naaman, Angew. Chem., Int. Ed. **53**, 8953 (2014).
[11] P. C. Mondal, N. Kantor-Uriel, S. P. Mathew, F. Tassinari, C. Fontanesi, and R. Naaman, Adv. Mater. **27**, 1924 (2015).
[12] A.-M. Guo and Q.-F. Sun, Phys. Rev. Lett. **108**, 218102 (2012).
[13] A.-M. Guo and Q.-F. Sun, Phys. Rev. B **86**, 115441 (2012).
[14] A.-M. Guo and Q.-F. Sun, Phys. Rev. B **86**, 035424 (2012).
[15] A.-M. Guo and Q.-F. Sun, Proc. Natl. Acad. Sci. USA **111**, 11658 (2014).
[16] T.-R. Pan, A.-M. Guo, and Q.-F. Sun, Phys. Rev. B **92**, 115418 (2015).
[17] A. A. Eremko and V. M. Loktev, Phys. Rev. B **88**, 165409 (2013).
[18] S. Matityahu, Y. Utsumi, A. Aharony, O. Entin-Wohlman, and C. A. Balseiro, Phys. Rev. B **93**, 075407 (2016).
[19] N. Hoffmann, Chem. Rev. **108**, 1052 (2008).
[20] S. D. Han, D. R. Anderson, A. D. Bond, H. V. Chu, R. L. Disch, D. Holmes, J. M. Schulman, S. J. Teat, K. P. C. Vollhardt, and G. D. Whitener, Angew. Chem., Int. Ed. **41**, 3227 (2002).
[21] Y. Shen and C.-F. Chen, Chem. Rev. **112**, 1463 (2011).
[22] M. Gingras, G. Félix, and R. Peresutti, Chem. Soc. Rev. **42**, 1007 (2013).
[23] K. Tanaka, H. Osuga, and Y. Kitahara, J. Chem. Soc. Perkin Trans. **2**, 2492 (2000).
[24] K. Tanaka, H. Osuga, and Y. Kitahara, J. Org. Chem. **67**, 1795 (2002).
[25] M. Newcomb, J. L. Toner, R. C. Helgeson, and D. J. Cram, J. Am. Chem. Soc. **101**, 4941 (1979).
[26] Y. Xu, Y. X. Zhang, H. Sugiyama, T. Umano, H. Osuga, and K. Tanaka, J. Am. Chem. Soc. **126**, 6566 (2004).
[27] K.-i. Shinohara, Y. Sannohe, S. Kaieda, K.-i. Tanaka, H. Osuga, H. Tahara, Y. Xu, T. Kawase, T. Bando, and H. Sugiyama, J. Am. Chem. Soc. **132**, 3778 (2010).
[28] R. Hassey, E. J. Swain, N. I. Hammer, D. Venkataraman, and M. D. Barnes, Science **314**, 1437 (2006).
[29] C. Kim, T. J. Marks, A. Facchetti, M. Schiavo, A. Bossi, S. Maiorana, E. Licandro, F. Todescato, S. Toffanin, M. Muccini, C. Graiff, and A. Tiripicchio, Org. Electron. **10**, 1511 (2009).
[30] Y. Zhou, T. Lei, L. Wang, J. Pei, Y. Cao, and J. Wang, Adv. Mater. **22**, 1484 (2010).
[31] J. R. Brandt, X. Wang, Y. Yang, A. J. Campbell, and M. J. Fuchter, J. Am. Chem. Soc. **138**, 9743 (2016).
[32] Y.-D. Guo, X.-H. Yan, Y. Xiao, and C.-S. Liu, Sci. Rep. **5**, 16731 (2015).
[33] J. Vacek, J. V. Chocholoušová, I. G. Stará, I. Starý, and Y. Dubi, Nanoscale **7**, 8793 (2015).
[34] V. Kiran, S. P. Mathew, S. R. Cohen, I. H. Delgado, J. Lacour, and R. Naaman, Adv. Mater. **28**, 1957 (2016).
[35] J. Navaza, G. Tsoucaris, G. le Bas, A. Navaza, and C. de Rango, Bull. Soc. Chim. Belg. **88**, 863 (1979).
[36] W. H. Laarhoven and W. J. C. Prinsen, Top. Curr. Chem. **125**, 63 (1984).
[37] *Electronic Transport in Mesoscopic Systems*, edited by S. Datta (Cambridge University Press, Cambridge, 1995).
[38] W. Long, Q.-F. Sun, and J. Wang, Phys. Rev. Lett. **101**, 166806 (2008).
[39] Q.-F. Sun, J. Wang, and H. Guo, Phys. Rev. B **71**, 165310 (2005).
[40] Q.-F. Sun and X. C. Xie, Phys. Rev. B **73**, 235301 (2006).
[41] Q.-F. Sun and X. C. Xie, Phys. Rev. B **71**, 155321 (2005).
[42] A.-M. Guo, E. Díaz, C. Gaul, R. Gutierrez, F. Domínguez-Adame, G. Cuniberti, and Q.-F. Sun, Phys. Rev. B **89**, 205434 (2014).